

Homolytic Cleavage of Fe–S Bonds in Rubredoxin under Mechanical Stress**

Guilherme M. Arantes,* Anirban Bhattacharjee, and Martin J. Field

The biosynthesis, stability, and folding pathways of the iron–sulfur proteins^[1,2] can be probed by analyzing protein unfolding and Fe–S bond dissociation. Some of the simplest iron–sulfur proteins belong to the rubredoxin family, which participate in electron transfer processes in bacteria and archaea. Rubredoxins lack inorganic sulfide and have only one Fe center coordinated by the side-chains of four cysteine residues^[2] (Figure 1a and b). Recent rubredoxin unfolding experiments, performed by protein engineering and single-molecule atomic-force microscopy,^[3,4] indicated that their Fe–S bonds had an unexpectedly low stability under mechanical stress. It was suggested that the activation process for bond

dissociation^[3] could occur by heterolytic fission, as observed for disulfide bridges,^[5] or homolytic cleavage, as hypothesized for the rupture of C–Si bonds.^[6] Given that Fe complexes can have near-degenerate levels with different total spin,^[7] an understanding of the reactivity of iron–sulfur clusters requires that their spin states and spin crossovers be characterized during the reaction.

Herein we have adopted a multiscale modeling approach employing quantum chemical (QC), molecular mechanical (MM), and hybrid QC/MM potentials, to address these questions. Full details of the models and programs used are given in the Supporting Information. We started by studying the mechanical unfolding of rubredoxin using an MM potential with an implicit model of solvent. A standard biomolecular force field was employed, except for the Fe–S bonds of the iron–sulfur complex which were represented by specially parameterized Morse potentials that permitted bond dissociation. The starting structures for all simulations were derived from those of the oxidized rubredoxin from *Pyrococcus furiosus* (protein databank (PDB) codes 1BRF and 1CAA^[9,10]). Unfolding was emulated by performing molecular dynamics (MD) simulations of the protein with an added harmonic potential that pulled apart the N- and C-termini at a constant speed.

Although we imposed no bias on the order of dissociation of the Fe–S bonds, we observed that the Fe–S(Cys5) bond ruptured first in most of our simulations. Results of one of these simulations carried out with a pulling speed of 10 nm ns⁻¹ are shown in Figure 2. It is clear from the C_α RMSDs that rubredoxin unfolds during the trajectory. The first contacts disrupted are interchain hydrogen bonds in the anti-parallel β-strand formed between the N- and C-termini. Other local polar contacts that stabilize the secondary structure are approximately maintained throughout the simulation, but fluctuations of the hydrophobic contacts and hydrogen bonds in the protein's core result in progressive disorganization of the globular fold. In the last part of the trajectory, the hydrogen bonds that hold together the N-terminal anti-parallel β-strand are broken. Large fluctuations are observed for both the Fe–S_γ bond distances (±0.5 Å) and S_γ–Fe–S_γ valence angles (±20°) along the trajectory, until the Fe–S_γ(Cys5) bond breaks after about 1 ns of simulation (Supporting Information Figure S1).^[8]

A snapshot of one of the unfolded rubredoxin structures obtained just before Fe–S_γ bond disruption is shown in Figure 1c. The local symmetry around the iron–sulfur center is broken upon mechanical unfolding with the iron tetrahedral coordination (pseudo-*T*_d) changing to *C*₂. This step is characterized by changes in the S_γ–Fe–S_γ valence angles from approximately 109° in folded rubredoxin to 90–125° in the

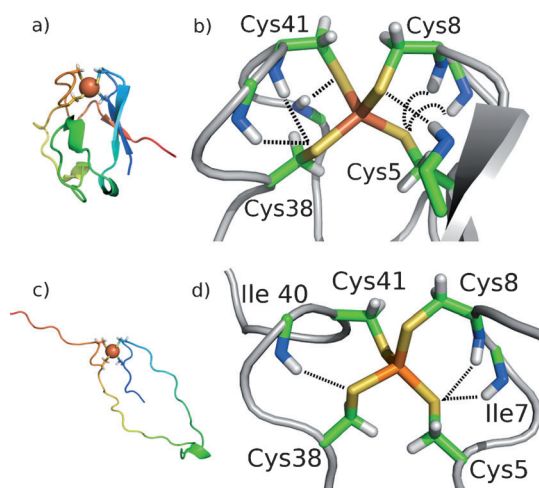


Figure 1. Rubredoxin structures: a) schematic representation of the folded protein; b) close-up of the iron–sulfur cluster from the folded protein; c) schematic representation of the protein from one of the pulling simulations just before Fe–S bond rupture; and d) close-up of the iron–sulfur cluster from the structure shown in (c). In (b) and (d) important hydrogen bonds are indicated by dashed lines and Fe orange, S yellow, C green, N blue.

[*] Dr. G. M. Arantes
Departamento de Bioquímica, Instituto de Química
Universidade de São Paulo
Av. Lineu Prestes 748, 05508-900, São Paulo, SP (Brazil)
E-mail: garantes@iq.usp.br

Dr. A. Bhattacharjee, Dr. M. J. Field
Institut de Biologie Structurale (IBS) Jean-Pierre Ebel
CEA/CNRS/Université Joseph Fourier
41, rue Jules Horowitz, 38027 Grenoble, Cedex 1 (France)

[**] We acknowledge funding from FAPESP (projects 07/52772-6 and 12/02501-4) and a joint FAPESP-CNRS project (23277).

Supporting information for this article is available on the WWW under <http://dx.doi.org/10.1002/anie.201303462>.

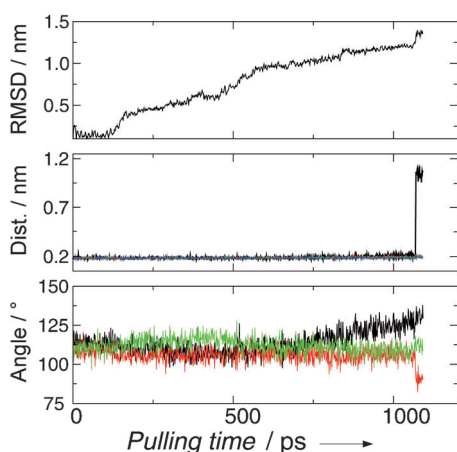


Figure 2. Structural changes during a rubredoxin pulling simulation. Top: the protein C_{α} root mean squared deviation (RMSD) from the initial folded structure; middle: the Fe–S distances for the Cys5 (black), Cys8 (red), Cys38 (green), and Cys41 (blue) side chains; bottom: the $S_{\gamma}(\text{Cys5})\text{--Fe--}S_{\gamma}$ valence angles for the Cys8 (black), Cys41 (red), and Cys38 (green) side chains.

unfolded protein (Tables S3 and S4).^[8] Hydrogen bonds in the vicinity of the iron–sulfur center are also significantly perturbed upon unfolding. The four backbone hydrogen bonds ($\text{O}\cdots\text{HN}$) involving Cys5 and Cys38 in the folded rubredoxin are disrupted as are three of the six hydrogen bonds between the protein backbone and the four S_{γ} s, with only the $S_{\gamma}(\text{Cys5})\cdots\text{NH}(\text{Cys8})$, $S_{\gamma}(\text{Cys5})\cdots\text{NH}(\text{Ile7})$, and $S_{\gamma}(\text{Cys38})\cdots\text{NH}(\text{Ile40})$ interactions maintained in the stretched protein (Figure 1 d and Tables S3 and S4^[8]).

To assess the effect of the rubredoxin environment on Fe–S stretching, we probed the intrinsic stability of Fe^{III}–thiolate bonds using density functional theory (DFT) calculations of the gas-phase model reaction [Eq. (1)].

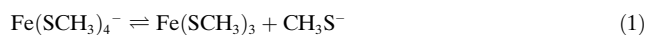


Figure 3a shows the energy profile for this reaction and Table S1^[8] some relevant geometrical parameters. From these it can be seen that the reactant, $\text{Fe}(\text{SCH}_3)_4^-$, has a sextet ground state and S_4 symmetry with local tetrahedral iron coordination, whereas the product, in which one Fe–S bond is broken, has a quartet ground state and C_2 symmetry. Doublet states were also considered but they were at least 50 kJ mol^{-1} higher in energy. The sextet profile has a late transition state (TS) whereas the quartet has an early TS. A minimum energy crossing point (MECP)^[11] between the energy surfaces of the two spin states was found just after the quartet TS along the reaction coordinate. This is the highest energy point along the pathway that connects sextet reactants to quartet products. The energetics of this MECP as well as the efficiency of spin crossover (given mostly by the magnitude of the spin-orbit coupling) are largely responsible for determining the kinetics of the intrinsic Fe–S dissociation reaction.

Spin populations for stationary points along the path are shown in Table S2^[8] which indicates that both quartet and sextet reactants may be described as formal $\text{Fe}^{\text{III}}\cdots\text{S}^{\text{II}-}$ or ferric–thiolate complexes given that the spin populations on

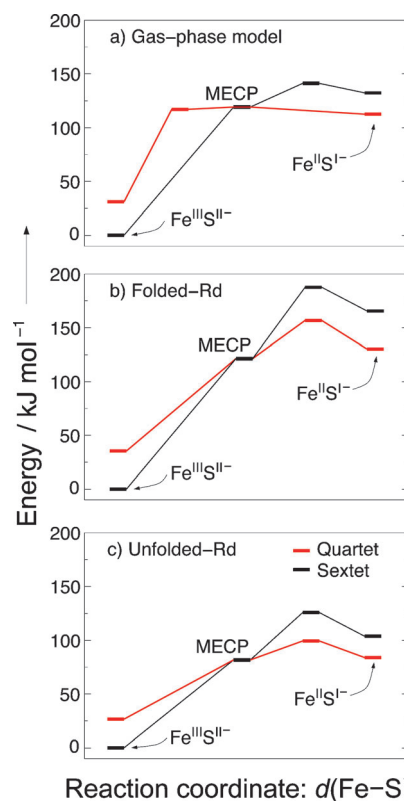


Figure 3. Relative energy profiles for iron–sulfur bond dissociation in the quartet (red) and sextet (black) spin states. Fe–S dissociation proceeds from left to right in all panels with the reaction coordinate taken as the Fe–S distance, $d(\text{Fe–S})$. a) the DFT profile for the gas-phase model Equation (1); b) and c) DFT/MM profiles for folded and unfolded rubredoxin (Rd), respectively.

the sulfur atoms are small. In contrast, the products have approximately one unpaired electron on the dissociated sulfur atom, suggesting a formal $\text{Fe}^{\text{II}}\cdots\text{S}^{\text{I}-}$ or a ferrous–thiolate radical pair. The spin populations of the intermediate points with increasingly higher Fe–S distance interpolate nicely between the $\text{Fe}^{\text{III}}\cdots\text{S}^{\text{II}-}$ and $\text{Fe}^{\text{II}}\cdots\text{S}^{\text{I}-}$ formal descriptions, indicating that Fe–S dissociation in $\text{Fe}(\text{SCH}_3)_4^-$ proceeds through a homolytic bond fission mechanism.

To examine Fe–S bond rupture in the protein, QC/MM calculations of the protein in explicit solvent were performed using structures obtained from the MM/MD simulations. In these models, the Fe center and Cys side-chains were in the QC region and were treated with a DFT potential. Only Fe–S(Cys5) rupture was studied in detail because there is experimental evidence that this and the Fe–S(Cys38) bond are the most labile of the four Cys bonds.^[3,4] Our simple mechanical model under stress also produced Fe–S(Cys5) dissociation in most of the pulling simulations that we conducted, and tests of Fe–S rupture calculated with the hybrid potential gave higher barriers for the other three Cys residues.

Figure 3b and c show that both folded and unfolded rubredoxin are similar to the gas-phase model with ground-state sextet reactants and quartet products. In contrast, the TSs on both surfaces are late, with the MECPs between the

surfaces coming before the TSs and 20–30 kJ mol⁻¹ lower in energy. This situation indicates that the Fe–S dissociation kinetics in rubredoxin will be mainly determined by the ⁴TS–⁶R energy difference. Spin crossover is still part of the reaction mechanism but should play a less-important kinetic role for dissociation in the protein compared to the intrinsic gas-phase reaction. The mechanism of bond fission is homolytic in both rubredoxin models. Spin populations (not shown) are similar to the gas-phase values, with both quartet and sextet products having approximately one unpaired electron on sulfur, indicating a Fe^{II}–thiolate radical dissociation product.

The protein environment imposes significant geometrical constraints on the cluster. The quartet–sextet gap increases by approximately 5 kJ mol⁻¹ in folded rubredoxin and decreases by about the same amount in unfolded rubredoxin compared to the gas-phase gap. The folded protein restricts Fe coordination to a rather symmetrical tetrahedral coordination (Tables S3,S4),^[8] which destabilizes the quartet state. On the other hand, unfolded rubredoxin is more flexible and allows the coordination around iron to relax. Consequently, reaction barriers and energies for both spin-states are significantly higher (ca. 50 kJ mol⁻¹, Figure 3 b and c) in folded rubredoxin as a result of constraints in Fe–S bond elongation imposed by the folded protein matrix.

These constraining effects are partially mitigated by hydrogen bonds between the S_γ atoms of the cluster and the protein backbone, especially S_γ(Cys5)⋯NH(Ile7) which is maintained throughout the reaction and stabilizes Fe–S rupture (Table S4).^[8] This type of hydrogen-bonding stabilization has been confirmed by experiments which show that mutation of Ile7 to Pro in rubredoxin results in greater Fe–S bond mechanical stability.^[4] The simulated reaction energy and barrier for the flexible unfolded rubredoxin are 20–30 kJ mol⁻¹ lower than the gas-phase reaction. Both hydrogen-bonding and protein constraints are responsible for shifting ⁴TS to a late TS in unfolded rubredoxin.

The barrier to Fe–S dissociation in unfolded rubredoxin is 99 kJ mol⁻¹ corresponding to the relative energy of ⁴TS (Figure 3 c). This compares reasonably well with the barrier of 78 kJ mol⁻¹ derived from the experimental dissociation rate (0.15 s⁻¹).^[3] The low barrier obtained for the reverse reaction, in which the Fe–S bond reforms (right to left on Figure 3 c), is also corroborated experimentally as the rubredoxin recovers mechanical stability upon relaxation of the stressed chain.^[3] This qualitative agreement provides support for the simulation methodology that we employ.

A high degree of covalency has been assigned to the Fe–S bond from the interpretation of X-ray absorption spectroscopy on iron–sulfur complexes,^[12] although it does not translate into a high stability for Fe–S bonds in rubredoxin

under mechanical stress.^[3] In the analysis proposed by Solomon et al.,^[12] the stability of a Fe–S bond depends on its covalency as well as on the electrostatic interaction energy between the dissociated fragments. For the homolytic reaction detected in our work, the radical products [Fe^{II}Cys₃⋯S⁻¹Cys] will have neutral formal charges and consequently a much smaller electrostatic interaction than charge separated heterolytic products. Thus, the mechanical stability of Fe–S bonds in stretched rubredoxin is principally determined by their intrinsic bond covalency and interactions with the protein matrix, with the ionic character of the bonds playing only a minor role.

Herein we have shown that iron–sulfur tetrahedral complexes have sextet ground states at their equilibrium geometries but pass through a spin crossing and change to quartet states upon Fe–S dissociation. This two-state reactivity has been extensively characterized in metal complexes^[7] and is relevant for the stability of Fe–S bonds in rubredoxin. For both folded and mechanically unfolded rubredoxin, and for the intrinsic reaction, Fe–S cleavage follows a homolytic mechanism. Such a mechanism, and the insights provided by our calculations, should be pertinent for studies of dissociation of metal–ligand bonds in other bioinorganic complexes and metalloenzymes.

Received: April 23, 2013

Published online: June 18, 2013

Keywords: density functional theory · iron–sulfur clusters · molecular dynamics · single-molecule studies · spin crossover

- [1] H. Beinert, R. H. Holm, E. Munck, *Science* **1997**, *277*, 653–659.
- [2] H. Beinert, *J. Biol. Inorg. Chem.* **2000**, *5*, 2–15.
- [3] P. Zheng, H. Li, *J. Am. Chem. Soc.* **2011**, *133*, 6791–6798.
- [4] P. Zheng, S. J. Takayama, A. G. Mauk, H. Li, *J. Am. Chem. Soc.* **2012**, *134*, 4124–4131.
- [5] S. Garcia-Manyes, J. Liang, R. Szożkiewicz, T.-L. Kuo, J. M. Fernandez, *Nat. Chem.* **2009**, *1*, 236–242.
- [6] M. Grandbois, M. Beyer, M. Rief, H. Clausen-Schaumann, H. E. Gaub, *Science* **1999**, *283*, 1727–1730.
- [7] D. Schröder, S. Shaik, H. Schwarz, *Acc. Chem. Res.* **2000**, *33*, 139–145.
- [8] Full details can be found in the Supporting Information.
- [9] R. Bau, D. C. Rees, D. M. Kurtz, R. A. Scott, H. Huang, M. W. W. Adams, M. K. Eidsness, *J. Biol. Inorg. Chem.* **1998**, *3*, 484–493.
- [10] M. W. Day, B. T. Hsu, L. Joshua-Tor, J. B. Park, Z. H. Zhou, M. W. Adams, D. C. Rees, *Protein Sci.* **1992**, *1*, 1494–1507.
- [11] S. Madsen, F. Jensen, *Theor. Chem. Acc.* **2009**, *123*, 477–485.
- [12] E. I. Solomon, S. I. Gorelsky, A. Dey, *J. Comput. Chem.* **2006**, *27*, 1415–1428.